Plasmon-induced optical control over dithionite-mediated chemical redox reactions

Junyang Huang, [iD] †[a] Bart de Nijs, [iD] †[a] Sean Cormier, [iD] [a]
Kamil Sokolowski, [iD] [b] David-Benjamin Grys, [iD] [a]
Charlie A. Readman, [iD] [b] Steven J. Barrow, [iD] [b] Oren A. Scherman [iD] [b]
and Jeremy J. Baumberg [iD] *[a]

External-stimuli controlled reversible formation of radical species is of great interest for synthetic and supramolecular chemistry, molecular machinery, as well as emerging technologies ranging from (photo)catalysis and photovoltaics to nanomedicine. Here we show a novel hybrid colloidal system for light-driven reversible reduction of chemical species that, on their own, do not respond to light. This is achieved by the unique combination of photo-sensitive plasmonic aggregates and temperature-responsive inorganic species generating radicals that can be finally accepted and stabilised by non-photo-responsive organic molecules. In this system Au nanoparticles (NPs) self-assembled via sub-nm precise molecular spacers (cucurbit[n]urils) interact strongly with visible light to locally accelerate the decomposition of dithionite species ($S_2O_4^{2-}$) close to the NP interfaces. This light-driven process leads to the generation of inorganic radicals whose electrons can then be reversibly picked up by small organic acceptors, such as the methyl viologen molecules (MV^{2+}) used here. During light-triggered plasmon- and heat-assisted generation of radicals, the $S_2O_4^{2-}$ species work as a chemical 'fuel' linking photo-induced processes at the NP interfaces with redox chemistry in the surrounding water environment. By incorporating MV^{2+} as a Raman-active reporter molecule, the resulting optically-controlled redox processes can be followed in real-time.

Introduction

Using light to control chemistry on the nanoscale has gathered much attention over recent years, for instance in light controlled molecular switching,[1]

[a]NanoPhotonics Centre, Cavendish Laboratory, Department of Physics, University of Cambridge, JJ Thompson Avenue, Cambridge, CB3 0HE, UK. E-mail: bd355@cam.ac.uk; jjb12@cam.ac.uk

[b]Melville Laboratory for Polymer Synthesis, Department of Chemistry, University of Cambridge, Lensfield Road, Cambridge CB2 1EW, UK

† These authors contributed equally.

optomechanics,[2] strong coupling,[3] and non-thermal plasmon-enhanced catalytic reactions,[4,5] all shown to be readily accessible using plasmonic nanoconstructs. Moreover, the ability to optically-control energy deposition through light absorption in plasmonic nanoconstructs is of great interest for emerging technologies providing a means to thermally activate localized (electro)chemical processes.[6–15] Such systems are of particular interest for their facile accessibility as they can be readily made using self-assembly, eliminating the need for expensive manufacturing processes, and typically proceed under ambient conditions.

Here, we present direct optical control over dithionite-mediated redox processes in aqueous environments using self-assembled gold nanoparticles (AuNPs). By self-assembling gold nanoparticles using either salt or sub-nm molecular spacers (cucurbit[n]urils: CB[n]), aggregates with broad spectral absorbance are formed. Both the AuNP aggregates assembled using salt or CB[n] can be utilized as efficient SERS substrates.[16–18] A redox reporter molecule such as methyl viologen (MV^{2+}) can be added to the substrates allowing for surface enhanced Raman spectroscopy (SERS) to be used to track *in situ* the dithionite redox processes in real-time.[17] We demonstrate that by switching between high and low laser irradiances, this reduction process can be turned on and off and the change in redox state of the reporter molecules can be directly observed. Such optical control over reduction opens up new avenues for switching (electro-)chemical processes, for example in fuel cells or batteries.

Results and discussion

Our hybrid system comprises (i) light-sensitive SERS-active Au nanoparticles self-assembled *via* sub-nm precise molecular spacers of CB[7] or by increasing the salt concentration, (ii) temperature-responsive inorganic dithionite species, $S_2O_4^{2-}$, and (iii) a non-photoresponsive organic electron-accepting molecule, MV^{2+}. The dithionite $S_2O_4^{2-}$ species in a water environment undergoes dissociation and complex transformations leading to a variety of free radicals, from which sulphur dioxide radical anions ($SO_2^{-\bullet}$) appear as the effective reducing agent in many redox reactions.[18] The dissociation of $S_2O_4^{2-}$ is temperature- and pH-dependent. At room temperature and neutral pH the formation of radical species can be thermally accelerated.[21] The redox potential of sulphur oxide radicals allows one-electron reduction of MV^{2+} leading to methyl viologen radical monocations, $MV^{+\bullet}$. Reduction of MV^{2+} is reversible in the presence of dioxygen, and in the case of chemical reduction by dithionite species can only appear once the concentration of sulphur dioxide radical anions is higher than that of dioxygen in a reaction environment ($[SO_2^{-\bullet}] > [O_2]$).[20,22] MV^{2+} was selected as the final electron acceptor on account of its characteristic Raman signatures for MV^{2+} and $MV^{+\bullet}$ species which allows one to distinguish between oxidized and reduced states and therefore easily track redox process dynamics by SERS.[19]

By adding cucurbit[n]uril to a colloidal suspension of citrate stabilized AuNPs, self-assembly forms aggregates with fractal-like structures,[23] red-shifting the plasmon resonance in extinction spectroscopy (Fig. 1a). As a result the extinction at 785 nm increases from 12% to 83% cm^{-1}. While a fraction of the extinction is plasmonic scattering, the remainder is converted to heat through non-radiative
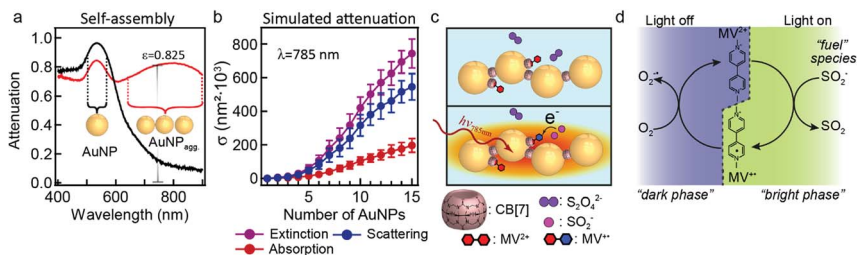
Fig. 1 Plasmonic-mediated chemistry. (a) Extinction spectra of the 60 nm AuNP suspension (black) and CB[7] spaced self-assembled AuNP aggregates (red) showing (b) 83% extinction per cm at 785 nm after 10 minutes of self-assembly. (c) Schematic illustration of thermally-activated dithionite reduction of MV^{2+}. (Top) At room temperature and ambient conditions reactions do not proceed, while (bottom) plasmon-induced heating catalyses dissociation and redox chemistry. (d) Scheme depicting the reduction and oxidation cycle of MV^{2+} by dithionite and oxygen, respectively.

relaxation processes in the Au (Fig. 1b). Such localized heating is used here to catalyse chemical reactions. The elevated temperatures accelerate the dissociation of the chemical 'fuel' $S_2O_4^{2-}$ species (Fig. 1c), leading to the formation of highly reactive $SO_2^{-\bullet}$ radical anions which efficiently reduce MV^{2+} molecules forming $MV^{+\bullet}$ radicals (Fig. 1d; bright phase). The high concentration of $MV^{+\bullet}$ radicals is maintained while the light is kept on and enough $S_2O_4^{2-}$ is present in the system. Once the light is switched off, $MV^{+\bullet}$ radicals are quickly re-oxidized by oxygen molecules, restoring the MV^{2+} (Fig. 1d; dark phase). The system is reversible and this cycle can be repeated until the $S_2O_4^{2-}$ fuel is consumed. Using a 785 nm laser to plasmonically induce the local temperature increase, the activated chemical redox processes can be followed in real time using surface enhanced Raman spectroscopy, giving a much better idea of the complexity involved in such redox systems.

After several seconds of 125 mW laser power irradiation at 785 nm a set of clear changes are observed in the SERS spectra. The appearance of the 1660, 1600, 1357, 1248, and 1025 cm^{-1} bands are characteristic of the cation $MV^{+\bullet}$ species being formed.[24] Upon lowering the laser irradiation intensity to 11 mW (so that SERS spectra can still be collected) the MV^{2+} spectrum returns after several seconds. This redox process is repeatable until the dithionite 'fuel' for the chemical reaction is depleted. The reduction process can also be reproduced through 'bulk' heating of the entire cuvette. The bulk solution temperature at which this reduction is seen in SERS switching is 29.3 °C, 9.3 °C above room temperature. Comparing the different SERS spectra we find that the low power (Fig. 2a) and low temperature (Fig. 2b) spectra closely match the powder Raman spectrum of MV^{2+} (Fig. 2e, black and grey traces), while the reduced state observed at 125 mW (Fig. 2a) and higher temperatures (Fig. 2b) show many similarities to each other but are distinctly different from the MV^{2+} spectrum (Fig. 2e, red and green traces, respectively). Slight differences in the spectra between optically- and temperature-induced reduction suggest variations in the local environment as a result of a potentially different dissociation mechanism of dithionite. Spectra acquired with CB[7]-mediated aggregates and salt induced aggregates for the reduced species have almost identical spectral features.
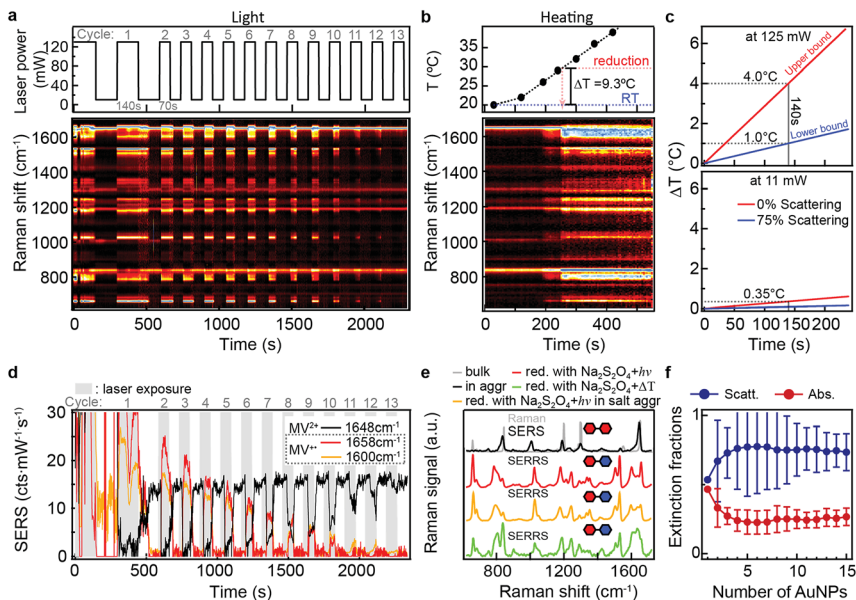
Faraday Discussions

Fig. 2 Optical switching and heat activation of the MV^{2+} redox process. Normalized SERS time scans of methyl viologen in the presence of sodium dithionite (a) under modulated irradiation power, and (b) with temperature ramping of the entire suspension. Both spectra are normalised by the integrated intensity from 1550 to 1700 cm^{-1}. (c) Calculated overall temperature change of the suspension caused by optical absorption with a laser power of 125 mW and 11 mW. Upper bound calculated assuming the incident light is fully absorbed by the AuNP aggregates, while the lower bound is calculated assuming 83% of irradiation at 785 nm is scattered. (d) Dynamics of SERS intensity of MV redox states (MV^{2+}: 1648 cm^{-1}, $MV^{+\bullet}$: 1658 cm^{-1}, 1600 cm^{-1}) under modulated laser power, with high laser exposure (125 mW) marked by shaded areas. (e) Raman spectra of the MV^{2+} solution with (black) and without (grey) the presence of AuNP aggregates, SERRS spectrum of $MV^{+\bullet}$ upon optically (red) and thermally (green) induced reduction with dithionite. (f) Calculated scattering and absorption fraction for different sized aggregates ranging from 1 to 15 AuNPs.

By considering the total laser power on the sample, an upper and lower estimate of the laser-induced bulk temperature increase per second can be estimated from

$$\Delta T = \frac{I_0 t \varepsilon_\lambda A}{C_Q m}, \qquad (1)$$

where I_0 is the incident laser intensity in J s^{-1}, t the duration of exposure, ε_λ the extinction of light over the optical path at the laser wavelength, A the fraction of absorbed light, C_Q the specific heat capacity and m the mass of water in the sample. Assuming all of the attenuated light is absorbed ($C_Q = 1$) an upper bound for ΔT is determined (red trace, Fig. 2c). Modelling the scattering properties of individual AuNP aggregates shows 25% absorbance and 75% scattering (Fig. 2f), providing a lower bound for ΔT ($C_Q = 0.25$). From this we find that the average temperature of the bulk suspension is increased by <4 °C after 140 s of laser irradiation at 125 mW.

In this estimate, heat dissipation to the surrounding environment is not considered, however the calculated ΔT_{max} is already insufficient to trigger the reduction by bulk temperature alone. The temperature increase of a single AuNP aggregate, ΔT_{agg}, due to optical absorption in a homogeneous medium can be estimated from

$$\Delta T_{\text{agg}} = \frac{\sigma_{\text{abs}} E_e}{4\pi R_{\text{eff}} \kappa_m}, \tag{2}$$

where σ_{abs} is the absorption cross section, E_e the incident irradiance of light, R_{eff} the effective radius of the aggregate,[25] and κ_m the thermal conductivity of the surrounding medium. For a simulated $\sigma_{\text{abs}} = 2 \times 10^5$ nm^2, $\kappa_{\text{water}} = 0.6$ W m^{-1} K^{-1}, and $R_{\text{eff}} = 160$ nm, we find an estimated average temperature increase of 1.6 °C on a single aggregate. Even if we consider only the gap region, which has a local plasmonic heating efficiency 1.5 times higher compared to the effective heating zone within 10 nm proximity from the aggregate, such a temperature increase is inadequate to reach $\Delta T_{\text{water}} > 9$ °C to catalyse the reduction process. This suggests that other local effects in the nanostructure play a key role in the catalysis of the reduction process. For example, the diffusion rate of oxygen molecules can be limited inside the confined gap regions, which in turn can allow the plasmonic heating to locally trigger the redox process at a lower temperature. Additionally, other optical or hot-electron effects on the chemistry process cannot be fully excluded at this stage.
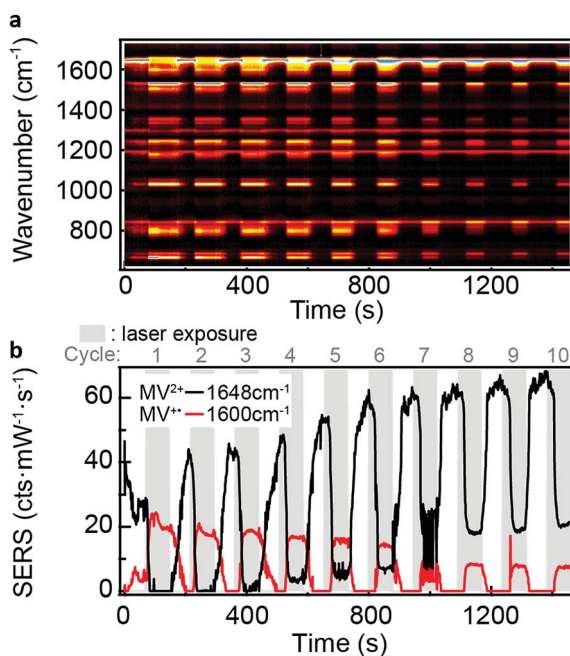

Fig. 3 Optical switching with salt induced AuNP aggregates. (a) Normalized SERS time scans of methyl viologen in the presence of sodium dithionite, under modulated irradiation power. (b) Correspondent SERS dynamics of MV redox states (MV^{2+}: 1648 cm^{-1}, MV$^{+\bullet}$: 1600 cm^{-1}), with high laser exposure (125 mW) marked by shaded areas.

Using salt to induce the AuNP aggregation yields a comparable switching phenomenon, however, two clear differences are observed (see Fig. 3). During the laser power modulation, the MV^{2+} signals continue to rise with each cycle, visible at the low powers . This contrasts with CB[7] in which a consistent peak amplitude is reached through each oxidation cycle. This is also in line with quantitative SERS results observed with CB[n] aggregates in literature.[17,18,26] The second notable difference is the faster (roughly two-fold) and more reliable redox switching observed for the salt induced aggregates. Switching with CB[5] formed aggregates is also investigated here, and comparable redox speeds are observed. However with CB[5], the aggregate-induced redox states are less stable, giving more fluctuating SERS signatures.

To investigate the switching behaviour with CB[7] and salt induced aggregates in more detail SERS signals extracted from the 1600 cm^{-1} ($MV^{+\bullet}$) and 1648 cm^{-1} (MV^{2+}) modes are compared between each reduction and oxidation cycle (Fig. 4a). By taking the first derivative peak this delay time can be plotted as a function of cycle number (Fig. 4b). To reach the triggering temperature of 29.3 °C for each cycle, the switching time is expected to occur faster on successive cycles as the
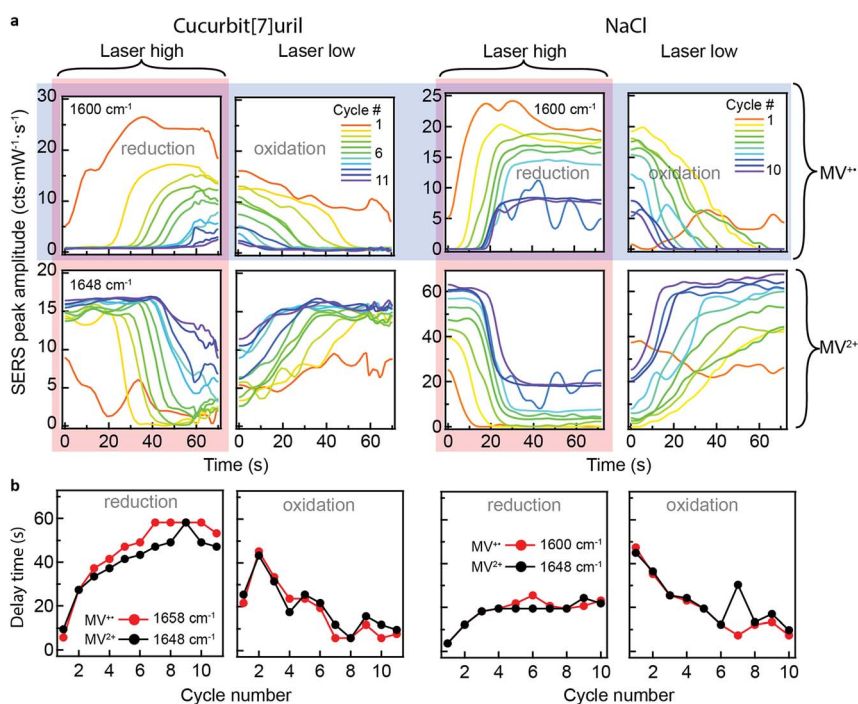

Fig. 4 Kinetics of the plasmon catalysed redox process with CB[7] and salt induced AuNP aggregates. (Left) CB[7] aggregates and (right) NaCl aggregates. (a) Evolution of SERS intensity of MV redox states for successive modulation cycles of laser power, with (top) the increase and decrease of the radical $MV^{+\bullet}$ species and (bottom) the correlated decrease and subsequent increase of the MV^{2+} species. (b) Extracted delay times of reduction and oxidation thresholds versus cycle number for high (left) CB[7] aggregates and (right) NaCl aggregates. The delay times are determined by the turning points of the first derivative of the SERS kinetics in (a).

solution accumulates heat. However, an opposite trend is observed in the case with CB[7] mediated aggregates. For these aggregates a clear increase in delay time for the reduction threshold is seen, whereas when salt is used to form aggregates, the delay time is shorter and after 3 cycles stabilises at 20 s. The re-oxidations of both systems show a comparable trend in which the oxidation process seems to consistently speed up with each cycle. These differences between the CB[7] and NaCl show that subtle variations in how the plasmonic substrates are formed can greatly affect the resulting switching behaviour suggesting that there is still much room for improvement. When fully developed, such a system can form a basis for promising radical-on-demand technologies.

Conclusions

We have demonstrated that plasmon-induced effects can be used to catalyse dithionite-mediated chemical reduction with either CB[7] or salt induced AuNP aggregates. By controlling irradiation intensities this reduction process can be switched on and off repeatably. We have shown that the localised effects close to the plasmonic aggregates is what causes redox switching, rather than bulk heating, and that the dithionite fuel controls the system response time.

Materials and methods

Dithionite was purchased from Sigma Aldrich, 60 nm citrate capped AuNPs were purchased from BBI solutions, and both were used as received. Cucurbit[n]uril spacer molecules were synthesized as described in ref. 27.

AuNP aggregates were assembled in an aqueous environment by mixing a CB[n] solution and a 60 nm citrate-capped colloidal AuNP suspension in a polystyrene cuvette (Fisher Scientific). For CB[n]-bridged aggregation, typically, 2 µL of 0.8 g L^{-1} CB[n] solution was first prepared in the cuvette and 1 mL of AuNP suspension was added to trigger the self-assembly process. After 1 min of CB[n] mediated aggregation, 3.6 µL of 0.1 g L^{-1} methyl viologen solution (Sigma-Aldrich) was mixed in to give $C_{CB[n]} : C_{MV}^{2+} = 1$. This was further followed by the addition of a small amount (0.1–0.2 mg) of sodium dithionite powder (Sigma-Aldrich) using a powder spatula. For salt induced aggregation, 10 µL of 5 molar NaCl solution was mixed with 1 mL of AuNP suspension, followed by the addition of 20 µL of 0.1 g L^{-1} methyl viologen solution and 0.2 mg of sodium dithionite powder.

The extinction, absorption, and scattering efficiencies of the AuNP clusters of varying size at a 785 nm wavelength are calculated using Mackowski's Multiple Sphere T-Matrix (MSTM, v3.0) code (available open source). The calculations use 100 iterations of randomly grown 60 nm gold nanoparticle cluster structures with defined inter-particle spacings (0.9 nm). The algorithm for generating the clusters consists of first adding a new AuNP onto the surface of the cluster from a randomized position and direction, and then allowing the new particle to relax to the nearest surface dimer at the specified interparticle distance (thus touching at least two other NPs). The randomly grown AuNP clusters are then surrounded with an external medium of water ($n = 1.33$). The dielectric function of the gold nanoparticles is interpolated from Johnson and Christy.

Raman spectroscopy was performed on a Renishaw inVia Raman microscope, using a 5× objective (NA = 0.12) and a 785 nm excitation diode laser. Such an excitation wavelength is known to resonantly excite the chain plasmons of the AuNP aggregates.[28,29] The laser beam was focused at the liquid–air interface from the top of the open cuvette (1 × 0.4 × 2.5 cm), without having the cuvette wall in the path of either the incident or scattered light. The spot size of the laser at the focal point with the 5× objective was measured to be 12 500 μm². Spectra were collected with a 1 s integration time and the irradiation power was alternated between 125 mW and 11 mW, where each power was maintained for 70 s. The optical depth of the suspension in the vertical direction was 2.5 cm. To control the temperature of the mixture the cuvette was placed in a water bath in contact with a hot plate. A thermometer was used to monitor the temperature of the water bath during the SERS measurement.

Conflicts of interest

There are no conflicts to declare.

Acknowledgements

References

1 Y. B. Zheng, *et al.*, Active Molecular Plasmonics: Controlling Plasmon Resonances with Molecular Switches, *Nano Lett.*, 2009, **9**, 819–825.

2 F. Benz, *et al.*, Single-molecule optomechanics in 'picocavities', *Science*, 2016, **354**, 726–729.

3 R. Chikkaraddy, *et al.*, Single-molecule strong coupling at room temperature in plasmonic nanocavities, *Nature*, 2016, **535**, 127–130.

4 X. Zhang, *et al.*, Plasmon-Enhanced Catalysis: Distinguishing Thermal and Nonthermal Effects, *Nano Lett.*, 2018, **18**, 1714–1723.

5 S. Mukherjee, *et al.*, Hot Electrons Do the Impossible: Plasmon-Induced Dissociation of H2 on Au, *Nano Lett.*, 2013, **13**, 240–247.

6 G. L. Liu, J. Kim, Y. Lu and L. P. Lee, Optofluidic control using photothermal nanoparticles, *Nat. Mater.*, 2006, **5**, 27–32.

7 A. M. Gobin, *et al.*, Near-Infrared Resonant Nanoshells for Combined Optical Imaging and Photothermal Cancer Therapy, *Nano Lett.*, 2007, **7**, 1929–1934.

8 P. K. Jain, I. H. El-Sayed and M. A. El-Sayed, Au nanoparticles target cancer, *Nano Today*, 2007, **2**, 18–29.

9 A. G. Skirtach, *et al.*, The Role of Metal Nanoparticles in Remote Release of Encapsulated Materials, *Nano Lett.*, 2005, **5**, 1371–1377.

10 D. Pissuwan, S. M. Valenzuela and M. B. Cortie, Therapeutic possibilities of plasmonically heated gold nanoparticles, *Trends Biotechnol.*, 2006, **24**, 62–67.

11 L. Wang and B. Li, Thermal Memory: A Storage of Phononic Information, *Phys. Rev. Lett.*, 2008, **101**, 267203.

12 L. Cao, D. N. Barsic, A. R. Guichard and M. L. Brongersma, Plasmon-Assisted Local Temperature Control to Pattern Individual Semiconductor Nanowires and Carbon Nanotubes, *Nano Lett.*, 2007, **7**, 3523–3527.

13 J. R. Adleman, D. A. Boyd, D. G. Goodwin and D. Psaltis, Heterogenous Catalysis Mediated by Plasmon Heating, *Nano Lett.*, 2009, **9**, 4417–4423.

14 S. Cormier, T. Ding, V. Turek and J. J. Baumberg, Actuating Single Nano-Oscillators with Light, *Adv. Opt. Mater.*, 2018, **6**, 1701281.

15 T. Ding, *et al.*, Light-induced actuating nanotransducers, *Proc. Natl. Acad. Sci. U. S. A.*, 2016, **113**, 5503–5507.

16 C. Andreou, M. R. Hoonejani, M. R. Barmi, M. Moskovits and C. D. Meinhart, Rapid Detection of Drugs of Abuse in Saliva Using Surface Enhanced Raman Spectroscopy and Microfluidics, *ACS Nano*, 2013, **7**, 7157–7164.

17 S. Kasera, L. O. Herrmann, J. del Barrio, J. J. Baumberg and O. A. Scherman, Quantitative multiplexing with nano-self-assemblies in SERS, *Sci. Rep.*, 2014, **4**, 6785.

18 B. de Nijs, *et al.*, Smart supramolecular sensing with cucurbit[*n*]urils: probing hydrogen bonding with SERS, *Faraday Discuss.*, 2017, **205**, 505–515.

19 B. Nijs, *et al.*, Plasmonic tunnel junctions for single-molecule redox chemistry, *Nat. Commun.*, 2017, **8**, 994.

20 K. Tsukahara and R. G. Wilkins, Kinetics of reduction of eight viologens by dithionite ion, *J. Am. Chem. Soc.*, 1985, **107**, 2632–2635.

21 R. G. Rinker, S. Lynn, D. M. Mason and W. H. Corcoran, Kinetics and Mechanism of Thermal Decomposition of Sodium Dithionite in Aqueous Solution, *Ind. Eng. Chem. Fundam.*, 1965, **4**, 282–288.

22 S. V. Makarov, E. V. Kudrik, R. van Eldik and E. V. Naidenko, Reactions of methyl viologen and nitrite with thiourea dioxide. New opportunities for an old reductant, *J. Chem. Soc., Dalton Trans.*, 2002, **0**, 4074–4076.

23 R. W. Taylor, *et al.*, Precise Subnanometer Plasmonic Junctions for SERS within Gold Nanoparticle Assemblies Using Cucurbit[*n*]uril 'Glue', *ACS Nano*, 2011, **5**, 3878–3887.

24 H. Feilchenfeld, G. Chumanov and T. M. Cotton, Photoreduction of Methylviologen Adsorbed on Silver, *J. Phys. Chem.*, 1996, **100**, 4937–4943.

25 G. Baffou, R. Quidant and F. J. García de Abajo, Nanoscale Control of Optical Heating in Complex Plasmonic Systems, *ACS Nano*, 2010, **4**, 709–716.

26 S. Kasera, F. Biedermann, J. J. Baumberg, O. A. Scherman and S. Mahajan, Quantitative SERS Using the Sequestration of Small Molecules Inside Precise Plasmonic Nanoconstructs, *Nano Lett.*, 2012, **12**, 5924–5928.

27 S. J. Barrow, S. Kasera, M. J. Rowland, J. del Barrio and O. A. Scherman, Cucurbituril-Based Molecular Recognition, *Chem. Rev.*, 2015, **115**, 12320–12406.

28 R. W. Taylor, R. Esteban, S. Mahajan, J. Aizpurua and J. J. Baumberg, Optimizing SERS from Gold Nanoparticle Clusters: Addressing the Near Field by an Embedded Chain Plasmon Model, *J. Phys. Chem. C*, 2016, **120**, 10512–10522.

29 C. Carnegie, *et al.*, Mapping SERS in CB:Au Plasmonic Nanoaggregates, *ACS Photonics*, 2017, **4**, 2681–2686.